PROCEEDINGS OF THE YEREVAN STATE UNIVERSITY

Physical and Mathematical Sciences 2022, **56**(3), p. 116–128

P h y s i c s

OPTICAL ABSORPTION IN SEMICONDUCTOR NANOWIRE MEDIATED BY ELECTRON-POLAR OPTICAL PHONON AND SPIN-ORBIT INTERACTIONS

T. K. GHUKASYAN

Chair of Solid States, YSU, Armenia

The intrasubband and intersubband absorption of light by free charge carriers in a semiconductor nanowire upon scattering by polar optical phonons mediated by Rashba and Dresselhaus spin-orbit interactions has been studied. The dependence of the absorption coefficient on the energy of the incident photon is investigated by counting the transitions between different conduction subbands. It is shown that the spin-orbit interaction leads to an increase in the coefficient of intrasubband and intersubband absorption of light, with the peaks of the absorption coefficient being determined by the energies of the absorbed photon and the absorbed or emitted phonon. In this case, the difference between the values of the absorption coefficients with or without spin-orbit interaction has maximum in the range of the local minimum of the absorption coefficient obtained by ignoring the spin-orbit coupling.

https://doi.org/10.46991/PYSU:A/2022.56.3.116

***Keywords*:** semiconductor nanowire, optical absorption, spin-orbit coupling, polar optical phonon.

Introduction. The study of the optical absorption coefficient (AC) with free carriers both in bulk semiconductors and in low-dimensional semiconductor structures makes it possible to determine the possible scattering mechanisms of free carriers [1] using the dependence of the optical absorption coefficient on temperature, the characteristic dimensions of low-dimensional structures, the intensity of external fields, etc.

The quantum theory of free carrier absorption (FCA) in bulk semiconductors for different scattering mechanisms is given in [2, 3]. FCA has been studied theoretically in semiconductor quantum wells (QW) and quantum well wires(QWR) when the electrons are scattered by acoustic phonons [1, 4–9], optical phonons [6, 10–14], and by other lattice imperfections.

* E-mail: tigran.ghukasyan@ysu.am

Spin-orbit coupling is a useful tool for controlling and manipulating spin degrees of freedom in solid-state systems [15]. In low-dimensional semiconductor structures, two types of spin-orbit coupling (SOC) are distinguished, which essentially depend on the size and shape of the nanostructure. The strength of the SOC associated with the asymmetry of the confining potential (Rashba SOC) [16] depends linearly on the momentum $\hbar k$ and is proportional to the magnitude of the applied electric field. Therefore, it can be controlled by an external gate voltage [17–20]. The SOC arising from the inversion asymmetry in a bulk crystal is called Dresselhaus SOC and has both a k-linear and a k-cubic terms [21]. The influence of the SOC on electron states [22–33] and related phenomena [34–39] in QWR have been successively studied experimentally and theoretically.

In this paper, for the first time, we take into account the simultaneous effect of the SOC and the confinement of polar optical phonons on the intrasubband and intersubband absorption of light in a nanowire. It is expected that the theoretical studies of both effects can be used for the potential applications of nanowires in high-speed-field devices.

Theory. We consider optical absorption in a cylindrical nanowire (NW) with radius r_0 and length L ($r_0 \ll L$) in an electric field $\boldsymbol{F}$ being perpendicular to the NW axis. It is assumed that the NW is made of a polar semiconductor material with static and high frequency dielectric constants ε_0 and ε_∞, respectively, and is embedded in a non-polar medium with dielectric constant ε_d. The confinement of the electron is modeled by the parabolic potential $V = m^*\omega_0^2 r^2/2$, where m^* is the effective mass of the electron and ω_0 is the potential frequency.

In [40] an expression for the free-carrier AC is obtained for the case when the radiation field is polarized parallel to the wire axis:

$$\gamma = \frac{8\alpha_{FS}}{n_r}\cdot\frac{\hbar\omega_0}{(\hbar\Omega)^3}\sum_{\substack{n,m,\mu\\ n',m'\\ j,\sigma}}\frac{\left(g^{j,\sigma}_{n'm',nm}\right)^2}{q}\left\{\left(N^j_\sigma+1\right)\left[\left(k^+-q\right)^2+\left(k^+\right)^2\right]f_{nm\mu}\left(k^+\right)\right.$$
$$\left.+N^j_\sigma\left[\left(k^-+q\right)^2+\left(k^-\right)^2\right]f_{nm\mu}\left(k^-\right)\right\}, \quad (1)$$

where n_r is the refractive index of the material, $\alpha_{FS} = e^2/\hbar c$ is the fine-structure constant, Ω is the frequency of the incident light, $n = n' = 0,1,2,\ldots$, $m = m' = 0,\pm1,\pm2,\ldots$, $\mu = \pm1$ are the quantum numbers of the electron, σ is the set of quantum numbers for a j-type phonon with $\sigma = (q,l,s)$ for $j =$ CO (confined optical) and $\sigma = (q,l)$ for $j =$ IO (interface optical), respectively, q is the component of the phonon wave vector in the direction of nanowire axis. N^j_σ is the equilibrium Bose–Einstein distribution function for polar optical phonons:

$$N^j_\sigma = \left[\exp\left(\frac{\hbar\omega^j_\sigma}{k_BT}\right)-1\right]^{-1}, \quad (2)$$

T is the temperature of the wire, $\hbar\omega^j_\sigma$ is the energy of a j-type phonon [41],

$$\omega_{\sigma}^{CO}=\sqrt{\frac{\varepsilon_0}{\varepsilon_{\infty}}}\omega_{TO}=\omega_{LO},\qquad \omega_{\sigma}^{IO}=\sqrt{1+\frac{\varepsilon_0-\varepsilon_{\infty}}{\varepsilon_{\infty}-\varepsilon(\omega)}}\omega_{TO}, \tag{3}$$

where

$$\varepsilon(\omega)=-\frac{I_l(qr_0)\left[K_{l-1}(qr_0)+K_{l+1}(qr_0)\right]}{K_l(qr_0)\left[I_{l-1}(qr_0)+I_{l+1}(qr_0)\right]}\varepsilon_d, \tag{4}$$

and $I_l(x)$ and $K_l(x)$ are the first and second kind modified Bessel functions, respectively. The distribution function $f_{nm\mu}(k)$ is given by

$$f_{nm\mu}(k)=\frac{2N_e\tanh\left(\frac{\hbar\omega_0}{2k_BT}\right)}{\left[1+\coth\left(\frac{\hbar\omega_0}{k_BT}\right)\right]}\sqrt{\frac{\pi\hbar^2}{2m^*k_BT}}\exp\left[-\frac{\hbar\omega_0(2n+|m|)}{k_BT}\right.$$
$$\left.-\frac{\hbar^2(k+\mu\frac{m^*}{\hbar^2}\sqrt{\alpha^2+\beta^2})^2}{2m^*k_BT}\right], \tag{5}$$

where N_e is the linear concentration of electrons in the wire, α and β are Rashba and Dresselhaus parameters in the absence of an applied electric field, respectively. The electron wave vector in case of the phonon absorption (k^-) and emission (k^+) is given by

$$k^{\pm}=\pm\frac{q}{2}-\mu\frac{m^*}{\hbar^2}\sqrt{\alpha^2+\beta^2}+\frac{m_e^*}{\hbar^2q}\left(\mp\hbar\Omega+\hbar\omega_{\sigma}^{j}\mp\Delta E_{nm}^{n'm'}\right), \tag{6}$$

where

$$E_{nm}^{n'm'}=\hbar\omega_0\left(2n-2n'+|m|-\left|m'\right|\right) \tag{7}$$

is the difference between the initial and final energy levels. $g_{n'm',nm}^{j,\sigma}$ in Eq. (1) is given by

$$g_{n'm',nm}^{j,\sigma}=\frac{1}{\pi r_0^2}\sqrt{\frac{n'!}{(n'+|m'|)!}\frac{n!}{(n+|m|)!}}\int_0^{2\pi}d\theta e^{-i(m'-m-l)\theta}\times$$
$$\times\int_0^{\infty}rdr\exp\left(-\rho^2\right)\rho^{|m'|+|m|}L_{n'}^{|m'|}\left(\rho^2\right)\Gamma_{\sigma}^{j}(r)L_n^{|m|}\left(\rho^2\right), \tag{8}$$

where

$$\rho=\frac{1}{r_0}\sqrt{r^2+r_F^2-2rr_F\cos\theta}, \tag{9}$$

$L_n^{|m|}(\rho)$ are the generalized Laguerre polynomials, $r_F=eF/\left(m^*\omega_0^2\right)$ and $\left|\Gamma_{\sigma}^{j}(r)\right|^2$ characterize the electron-phonon interaction strength [41].

Numerical Results. The intersubband AC in the NW is influenced by the spatial confinement, the electric field as well the Rashba and Dresselhaus SOC parameters. The main aim of this section is to clarify the role of each of the above-mentioned factors in determining the total AC.

Calculations have been performed for a free standing CdSe quantum wire with physical parameters $m^*=0.13m_0$ (m_0 is the electron mass), $\varepsilon_0=9.56$, $\varepsilon_{\infty}=6.23$, $\hbar\omega_{LO}=26.46\,meV$, $\hbar\omega_{TO}=21.36\,meV$ and $\alpha=\beta=4.5\cdot10^{-9}eV\cdot cm$.

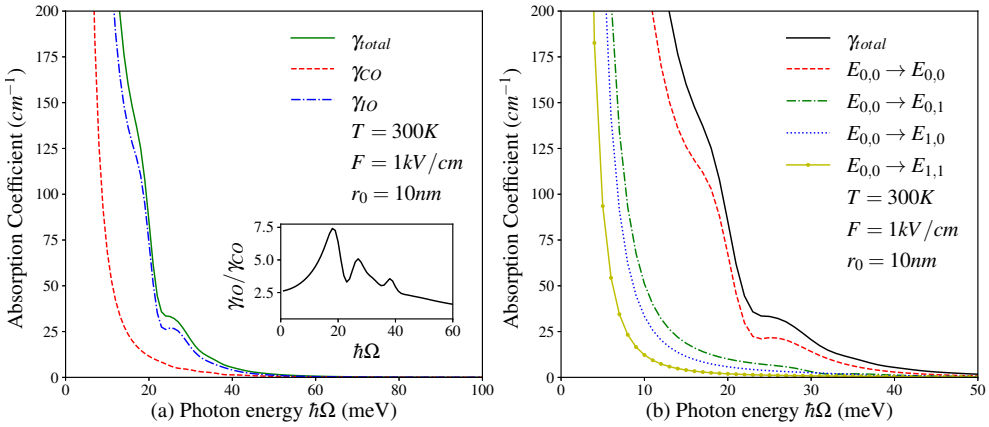

Fig. 1. (Color online) AC as a function of photon energy, $\hbar\Omega$, at $T = 300\ K$, $F = 1\ kV/cm$ and $r_0 = 10\ nm$. (a) The dash-dotted (blue) line shows the contribution of the IO phonons in the AC, the dashed (red) line shows the contribution of CO phonons in the AC, while the solid (green) line corresponds to the total AC. (b) The dashed (red) line corresponds to the intrasubband transitions, the dash-dotted (green) line corresponds to $E_{0,0} \to E_{0,1}$ transitions, the dotted (blue) line corresponds to the transition $E_{0,0} \to E_{1,0}$ while the line with points (yellow) corresponds to transitions $E_{0,0} \to E_{1,1}$.

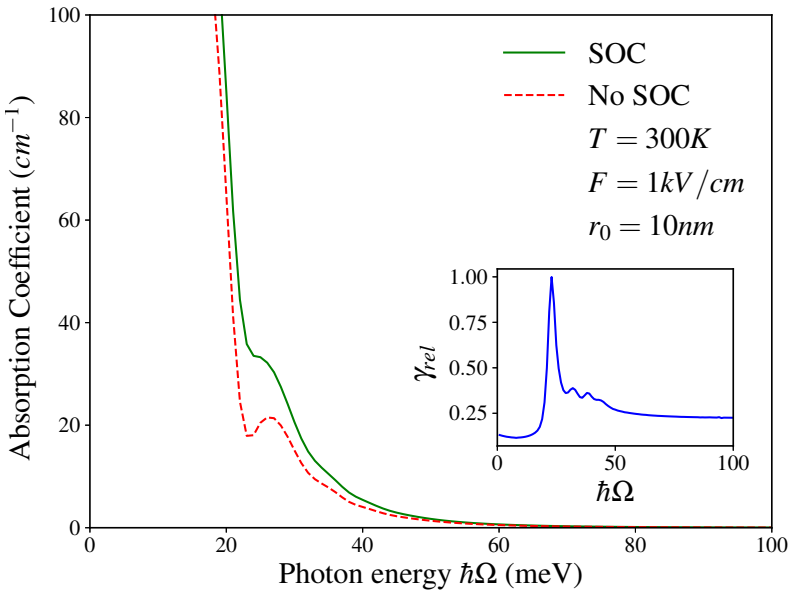

Fig. 2. (Color online) AC as a function of photon energy $\hbar\Omega$ at $T = 300\ K$, $F = 1\ kV/cm$, $r_0 = 10\ nm$, with taking into account and neglecting the SOC. The inset shows the relative AC, $\Delta\gamma_{rel} = (\gamma - \gamma_0)/\gamma_0$.

The contributions of CO and IO phonons in the total AC is presented as a function of photon energy (Fig. 1 (a)). It can be seen that the contribution of IO phonons in the total AC prevails over CO phonons, which is a consequence of the small radius of the wire. The inset of Fig. 1 (a) shows the relation of IO and CO phonon

contributions (γ_{IO}/γ_{CO}). Three distinct peaks are observed at photon energies 18 meV, 27 meV and 38 meV. The first two peaks are the result of phonon assisted intrasubband transitions, while the third peak coincides with the phonon assisted transition $E_{0,0} \to E_{1,0}$, because the transition energy is determined by $\Delta E_{0,0}^{1,0} + \hbar\omega_j = 37\ meV$. This indicates that for the $E_{0,0} \to E_{1,0}$ transition the emission of IO phonons is favored. The contributions of intrasubband and intersubband transitions are presented in Fig. 1 (b). It can be seen that the transitions to the lower energy subbands have more significant contributions in the total AC relative to transitions to the higher energy subbands, meanwhile the intrasubband transition leads to the most significant contribution. It should also be noted that each of the considered transitions has peaks at energies corresponding to phonon-assisted transitions, which, however, do not appear in the total AC due to their relative smallness.

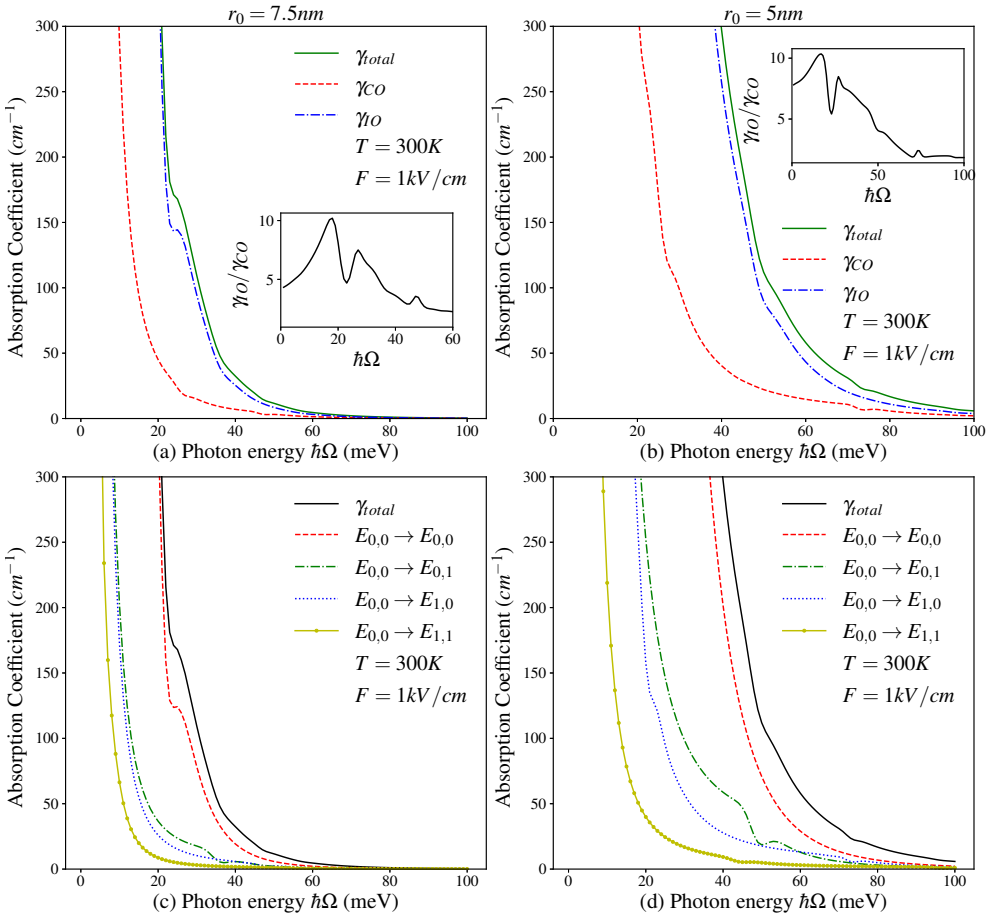

Fig. 3. (Color online) AC as a function of photon energy $\hbar\Omega$ at $T = 300\ K$, $F = 1\ kV/cm$ for wire radiuses $r_0 = 7.5\ nm$ ((a) and (c)) and $r_0 = 5\ nm$ ((b) and (d)). (a) and (c) show the contribution of IO and CO phonon interactions in the total AC, while in (c) and (d) the contribution of different subband transitions are presented.

Fig. 2 shows the dependence of the AC on the photon energy both taking into account and neglecting the SOC. An increase in the AC can be observed for all transitions when the SOC is taken into account. In the inset of Fig. 2 we present $\Delta\gamma_{rel} = (\gamma - \gamma_0)/\gamma_0$. It can be seen from the inset that $\Delta\gamma$ reaches its maximum at the local minimum near the AC peak.

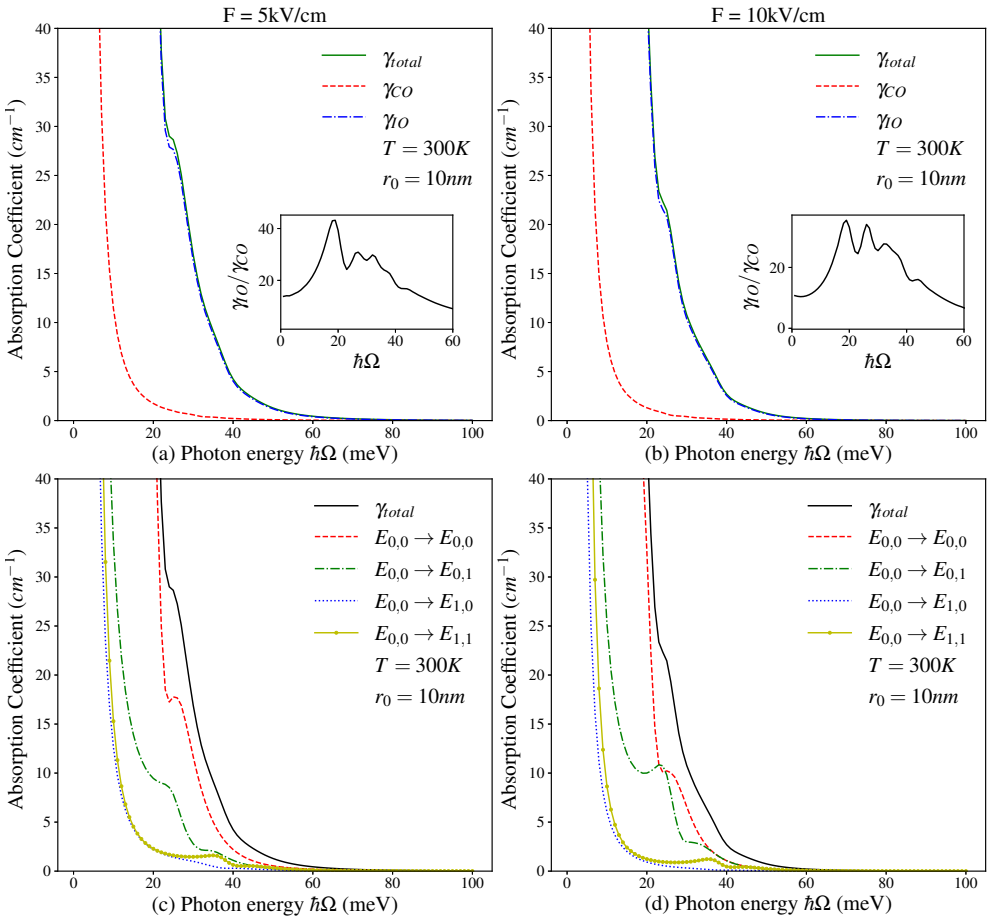

Fig. 4. (Color online) AC as a function of photon energy $\hbar\Omega$ at $T = 300\ K$, $r_0 = 10\ nm$ for electric field strengths $F = 5\ kV/cm$((a) and (c)) and $F = 10\ kV/cm$ ((b) and (d)). (a) and (c) show the contribution of IO and CO phonon interactions in the total AC, while in (c) and (d) the contribution of different subband transitions are presented.

Additionally, we have studied the AC of a nanowire as a function of photon energy for wire radii $r_0 = 7.5\ nm$ and $r_0 = 5\ nm$ (Fig. 3). The contribution of IO and CO phonons as well as their ratio γ_{IO}/γ_{CO} (inset) is presented in Fig. 3 (a) and (b), while Fig. 3 (c) and (d) show the contributions in AC due to transitions between different energy subbands. It can be seen in Fig. 3 (a) and (b), that decreasing the wire radius leads to an increase in the AC, both for IO and CO scattering. It is also worth mentioning that in these cases too, three distinct peaks are observed for the ratio of IO and CO contributions. The energies for the first two peaks are the same as in case of

$r_0 = 10\ nm$, while the energy of the third peak varies with the wire radius, remaining equal to the $E_{0,0} \to E_{1,0}$ transition energy. Furthermore, the AC curves obtained for electronic transitions between different subbands (Fig. 3 (c) and (d)) move away from each other with a decrease of wire radius which is a consequence of an increase of intersubband energies.

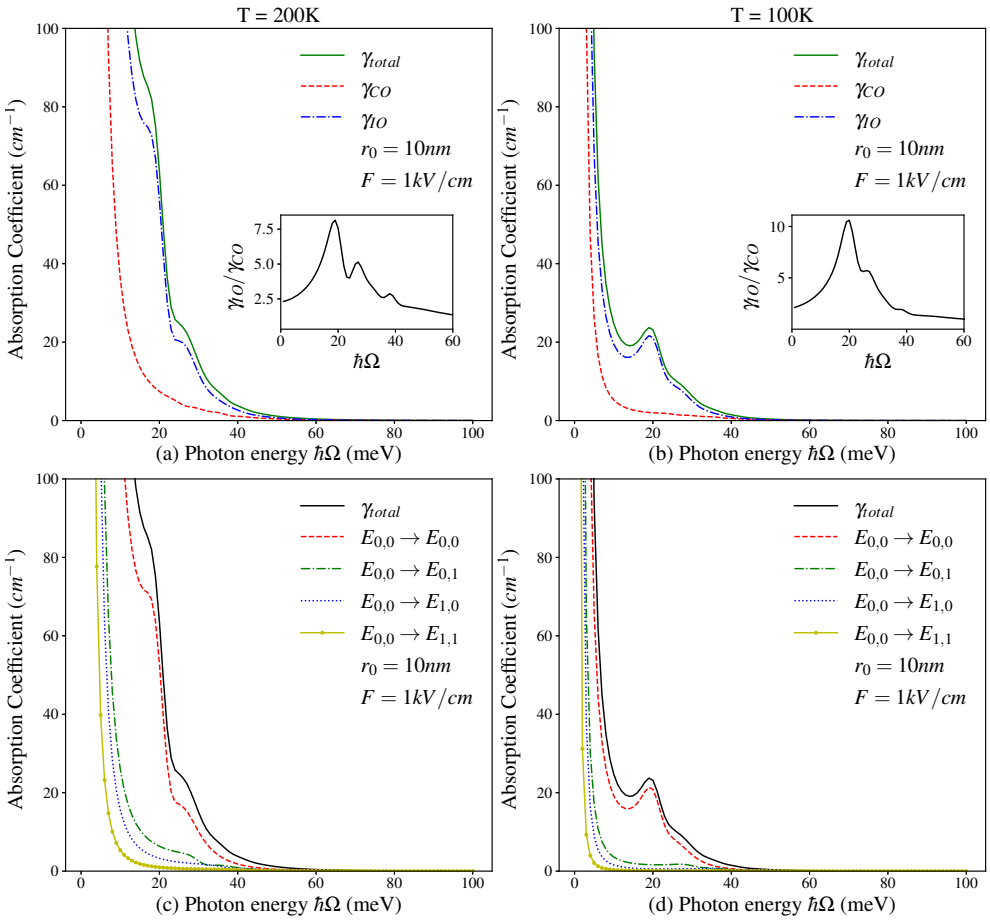

Fig. 5. (Color online) AC as a function of photon energy $\hbar\Omega$ at $F = 1\ kV/cm$, $r_0 = 10\ nm$ for temperatures $T = 200\ K$ ((a) and (c)) and $T = 100\ K$ ((b) and (d)). (a) and (c) show the contribution of IO and CO phonon interactions in the total AC, while in (c) and (d) the contribution of different subband transitions are presented.

We have also studied the AC for electric fields with strengths $F = 5\ kV/cm$ and $F = 10\ kV/cm$ (Fig. 4). As above, the contributions of IO and CO phonons and their ratio γ_{IO}/γ_{CO}, as well as the contributions in AC due to transitions between different energy subbands are calculated. It is evident that the increase of the electric field strength leads to an increase in the ratio γ_{IO}/γ_{CO}. This is a consequence of the fact that an increase of the electric field strength shifts the peak of the electron density distribution to the wire surface. In particular, the contribution of IO phonons is about 15 times greater than the contribution of CO phonons at $T = 300\ K$ and

$r_0 = 10\ nm$. It is interesting to note, that an increase of the electric field strength more significantly increases the contribution to the AC due to transition from subband $E_{0,0}$ to the subbands with $m = 1$ than from $E_{0,0}$ to the subbands with $m = 0$.

Finally, in Fig. 5 the AC as a function of photon energy is presented for temperatures $T = 100\ K$ and $T = 200\ K$. It can be seen that the decrease of temperature leads to a decrease in the AC. This is a consequence of the decrease of the average number of IO and CO phonons. Furthermore, at $T = 100\ K$ and $\hbar\Omega = 1\ meV$ a peak in the AC is observed, corresponding to phonon assisted transitions. The appearance of the peak with decreasing temperature indicates that it is caused by scattering on IO phonons, as their average number relatively increases with decreasing temperature.

Conclusion. In conclusion, the numerical calculations of the intersubband optical absorption of light in a semiconductor nanowire due to electron scattering by confined polar optical and interface polar optical phonons and taking into account the spin-orbit coupling were carried out. Both separately and in total, the contribution of electron scattering by both confined and interface optical phonons is presented in the dependences of the absorption coefficient on the photon energy. The roles of the wire radius, temperature and electric field strength have been studied. It has been shown that:

(i) the contribution of IO phonons in the total AC prevails over CO phonons, which is a consequence of the small radius of the wire;

(ii) the transitions to the lower energy subbands have more significant contributions in the total AC relative to transitions to the higher energy subbands;

(iii) the first two peaks in the ratio γ_{IO}/γ_{CO} correspond to intrasubband transitions, while the third peak corresponds to the phonon assisted $E_{0,0} \to E_{1,0}$ transition;

(iv) decreasing the wire radius leads to an increase in the AC, both for IO and CO scattering;

(v) an increase in the electric field strength more significantly increases the contribution to the AC due to transition from subband $E_{0,0}$ to the subbands with $m = 1$ than from $E_{0,0}$ to the subband with $m = 0$ and

(vi) at $T = 100\ K$ and $\hbar\Omega = 19\ meV$ a peak in the AC is observed, corresponding to phonon assisted transitions

We expect that the obtained results will be useful for further study of optical phenomena in a nanowire considering both the spin-orbit coupling and phonon confinement.

The author is grateful to prof. A. Vartanian and prof. A. Kirakosyan for the helpful discussion and valuable advices. The work was supported by the Science Committee of RA, in the frame of the research projects No. 21AA-1C021 and No. 21AG-1C048.

Received 29.06.2022
Reviewed 29.07.2022
Accepted 29.08.2022

REFERENCES

1. Bhargavi K.S., Patil S., Kubakaddi S.S. Acoustic Phonon Assisted Free-carrier Optical Absorption in an *n*-type Monolayer MoS2 and Other Transition-metal Dichalcogenides. *J. Appl. Phys.* **118** (2015), 044308. https://doi.org/10.1063/1.4927630
2. Dumke W.P. Quantum Theory of Free Carrier Absorption. *Phys. Rev.* **124** (1961), 1813–1817. https://doi.org/10.1103/physrev.124.1813
3. Seeger K. *Semiconductor Physics*. Springer, Berlin-Heidelberg (2004). https://doi.org/10.1007/978-3-662-09855-4
4. Spector H.N. Free-carrier Absorption in Quasi-two-dimensional Semiconducting Structures. *Phys. Rev. B* **28** (1983), 971–976. https://doi.org/10.1103/physrevb.28.971
5. Kubakaddi S.S., Mulimani B.G. Free-carrier Absorption in Semiconducting Quantum Well Wires. *J. Phys. C: Solid State Phys.* **18** (1985), 6647–6652. https://doi.org/10.1088/0022-3719/18/36/019
6. Adamska H., Spector H.N. Free-carrier Absorption from Electrons in Confined Systems. *J. Appl. Phys.* **59** (1986), 619–626. https://doi.org/10.1063/1.336621
7. Wu C.C., Lin C.J. Free-carrier Absorption in *n*-type Piezoelectric Semiconductor Films. *J. Phys. Condens. Matter* **6** (1994), 10147–10158. https://doi.org/10.1088/0953-8984/6/46/030
8. Yu Y.B., Zhu S.N., Guo K.X. Electron–phonon Interaction Effect on Optical Absorption in Cylindrical Quantum Wires. *Solid State Commun.* **139** (2006), 76–79. https://doi.org/10.1016/j.ssc.2006.04.009
9. Wu C.C., Lin C.J. Effect of Electron–phonon Scattering Mechanisms on Free-carrier Absorption in Quasi-one-dimensional Structures. *Physica B: Condens. Matter.* **316–317** (2002), 346–349. https://doi.org/10.1016/s0921-4526(02)00504-5
10. Adamska H., Spector H.N. Free Carrier Absorption in Quantum Well Structures for Polar Optical Phonon Scattering. *J. Appl. Phys.* **56** (1984), 1123–1127. https://doi.org/10.1063/1.334084
11. Wu C.C., Lin C.-J. Free-carrier Absorption in *n*-type Gallium Arsenide Films for Polar Optical Phonon Scattering. *J. Appl. Phys.* **79** (1996), 781–785. https://doi.org/10.1063/1.360825
12. Kubakaddi S.S., Mulimani B.G. Free-carrier Absorption in Quasi-two-dimensional Semiconducting Structures for Nonpolar Optical Phonon Scattering. *J. Appl. Phys.* **58** (1985), 3640–3642. https://doi.org/10.1063/1.335745
13. Kubakaddi S.S., Mulimani B.G. Free-carrier Absorption in Semiconducting Quantum-well Wires for Nonpolar Optical-phonon Scattering. *J. Appl. Phys.* **63** (1988), 1799–1801. https://doi.org/10.1063/1.339873
14. Khoa D.Q., Phuong L.T.T., Hoi B.D. Nonlinear Absorption Coefficient and Optically Detected Electrophonon Resonance in Cylindrical GaAs/AlAs Quantum Wires with Different Confined Phonon Models. *Superlattices Microstruct.* **103** (2017), 252–261. https://doi.org/10.1016/j.spmi.2017.01.025

15. Žutić I., Fabian J., Sarma S.D. Spintronics: Fundamentals and Applications. *Rev. Mod. Phys.* **76** (2004), 323–410.
https://doi.org/10.1103/revmodphys.76.323
16. Rashba E.I. *Fiz. Tver. Tela* **2** (1960), 1224 (in Russian).
17. Nitta J., Akazaki T., et al. Gate Control of Spin–orbit Interaction in an Inverted $In_{0.53}Ga_{0.47}As/In_{0.52}Al_{0.48}As$ Heterostructure. *Phys. Rev. Lett.* **78** (1997), 1335–1338.
https://doi.org/10.1103/physrevlett.78.1335
18. Grundler D. Large Rashba Splitting in InAs Quantum Wells Due to Electron Wave Function Penetration into the Barrier Layers. *Phys. Rev. Lett.* **84** (2000), 6074–6077.
https://doi.org/10.1103/physrevlett.84.6074
19. Koga T., Nitta J., et al. Rashba Spin–orbit Coupling Probed by the Weak Antilocalization Analysis in InAlAs/InGaAs/InAlAs Quantum Wells as a Function of Quantum Well Asymmetry. *Phys. Rev. Lett.* **89** (2002), 046801.
https://doi.org/10.1103/physrevlett.89.046801
20. Zhang S., Tang N., et al. Generation of Rashba Spin–orbit Coupling in CdSe Nanowire by Ionic Liquid Gate. *Nano Letters* **15** (2015), 1152–1157.
https://doi.org/10.1021/nl504225c
21. Dresselhaus G. Spin–orbit Coupling Effects in Zinc Blende Structures. *Phys. Rev.* **100** (1955), 580–586.
https://doi.org/10.1103/physrev.100.580
22. Knobbe J., Schäpers T. Magnetosubbands of Semiconductor Quantum Wires with Rashba Spin–orbit Coupling. *Phys. Rev. B* **71** (2005), 035311.
https://doi.org/10.1103/physrevb.71.035311
23. Serra L., Sánchez D., López R. Evanescent States in Quantum Wires with Rashba Spin–orbit Coupling. *Phys. Rev. B* **76** (2007), 045339.
https://doi.org/10.1103/physrevb.76.045339
24. Erlingsson S.I., Egues J.C., Loss D. Energy Spectra for Quantum Wires and Two-dimensional Electron Gases in Magnetic Fields with Rashba and Dresselhaus Spin–orbit Interactions. *Phys. Rev. B* **82** (2010), 155456.
https://doi.org/10.1103/physrevb.82.155456
25. Debald S., Kramer B. Rashba Effect and Magnetic Field in Semiconductor Quantum Wires. *Phys. Rev. B* **71** (2005), 115322.
https://doi.org/10.1103/physrevb.71.115322
26. Biswas T., Ghosh T.K. Electron–phonon Interaction in a Spin–orbit Coupled Quantum Wire with a Gap. *Semicond. Sci. Technol.* **30** (2014), 015022.
https://doi.org/10.1088/0268-1242/30/1/015022
27. Quay C.H.L., Hughes T.L., et al. Observation of a One-dimensional Spin–orbit Gap in a Quantum Wire. *Nat. Phys.* **6** (2010), 336–339.
https://doi.org/10.1038/nphys1626
28. Pereira R.G., Miranda E. Magnetically Controlled Impurities in Quantum Wires with Strong Rashba Coupling. *Phys. Rev. B* **71** (2005), 085318.
https://doi.org/10.1103/physrevb.71.085318
29. Karaaslan Y., Gisi B., et al. Spin–orbit Interaction and Magnetic Field Effects on the Energy Dispersion of Double Quantum Wire. *Superlattices Microstruct.* **85** (2015), 401–409.
https://doi.org/10.1016/j.spmi.2015.06.002
30. Serra L., Sánchez D., López R. Rashba Interaction in Quantum Wires with in-plane Magnetic Fields. *Phys. Rev. B* **72** (2005), 235309.
https://doi.org/10.1103/physrevb.72.235309

31. Song T.L., Liang X.X. Stark Effects on Bound Polarons in Polar Rectangular Quantum Wires. *J. Appl. Phys.* **110** (2011), 063721.
https://doi.org/10.1063/1.3642973
32. Zhang S., Liang R., et al. Magnetosubbands of Semiconductor Quantum Wires with Rashba and Dresselhaus Spin–orbit Coupling. *Phys. Rev. B* **73** (2006), 155316.
https://doi.org/10.1103/physrevb.73.155316
33. Zhang T.Y., Zhao W., Liu X.-M. Energy Dispersion of the Electrosubbands in Parabolic Confining Quantum Wires: Interplay of Rashba, Dresselhaus, Lateral Spin–orbit Interaction and the Zeeman Effect. *J. Phys. Condens. Matter* **21** (2009), 335501.
https://doi.org/10.1088/0953-8984/21/33/335501
34. Liu J.F., Zhong Z.C., et al. Enhancement of Polarization in a Spin–orbit Coupling Quantum Wire with a Constriction. *Phys. Rev. B* **76** (2007), 195304.
https://doi.org/10.1103/physrevb.76.195304
35. Governale M., Zülicke U. Spin Accumulation in Quantum Wires with Strong Rashba Spin–orbit Coupling. *Phys. Rev. B* **66** (2002), 073311.
https://doi.org/10.1103/physrevb.66.073311
36. Lee H.C., Yang S.-R.E. Collective Excitation of Quantum Wires and Effect of Spin–orbit Coupling in the Presence of a Magnetic Field Along the Wire. *Phys. Rev. B* **72** (2005), 245338.
https://doi.org/10.1103/physrevb.72.245338
37. Vartanian A., Kirakosyan A., Vardanyan K. Fröhlich Polaron in Nanowire with Rashba and Dresselhaus Spin–orbit Couplings. *Superlattices Microstruct.* **109** (2017), 655–661.
https://doi.org/10.1016/j.spmi.2017.05.057
38. Mireles F., Kirczenow G. Ballistic Spin-polarized Transport and Rashba Spin Precession in Semiconductor Nanowires. *Phys. Rev. B* **64** (2001), 024426.
https://doi.org/10.1103/physrevb.64.024426
39. Schäpers T., Knobbe J., Guzenko V.A. Effect of Rashba Spin-orbit Coupling on Magnetotransport in InGaAs/InP Quantum Wire Structures. *Phys. Rev. B* **69** (2004), 235323.
https://doi.org/10.1103/physrevb.69.235323
40. Vartanian A., Ghukasyan T., et al. Simultaneous Effects of the Confinement of Polar Optical Phonons and Spin–orbit Coupling on the Free Carrier Absorption of a Nanowire. *Micro and Nanostructures* **168** (2022), 207287.
https://doi.org/10.1016/j.micrna.2022.207287
41. Xie H.-J., Chen C.-Y., Ma B.-K. Bound Polaron in a Cylindrical Quantum Wire of a Polar Crystal. *Phys. Rev. B* **61** (2000), 4827–4834.
https://doi.org/10.1103/physrevb.61.4827

Տ. Կ. ՂՈՒԿԱՍՅԱՆ

ԷԼԵԿՏՐՈՆ-ԲԵՎԵՌԱՅԻՆ ՕՊՏԻԿԱԿԱՆ ՖՈՆՈՆ ԵՎ ՍՊԻՆ-ՈՒՂԵԾՐԱՅԻՆ ՓՈԽԱԶԴԵՑՈՒԹՅՈՒՆՆԵՐՈՎ ՊԱՅՄԱՆԱՎՈՐՎԱԾ ՕՊՏԻԿԱԿԱՆ ԿԼԱՆՈՒՄ ԿԻՍԱՀՂՈՐԴՉԱՅԻՆ ՆԱՆՈԼԱՐՈՒՄ

Ուսումնասիրվել է կիսահաղորդչային նանոլարում լույսի ներենթազոտային և միջենթազոտային կլանումը, պայմանավորված ազատ լիցքակիրների՝ բևեռային օպտիկական ֆոնոնների վրա ցրումներով և Ռաշբայի և Դրեսելհաուսի սպին-ուղեծրային փոխազդեցություններով: Հետազոտվել է կլանման գործակցի կախումը ընկնող ֆոտոնի էներգիայից՝ հաղորդականության տարբեր ենթազոտիների միջև անցումների հաշվառմամբ: Ցույց է տրվել, որ սպին-ուղեծրային փոխազդեցությունը հանգեցնում է լույսի ներենթազոտային և միջենթազոտային կլանման գործակցի աճի, իսկ կլանման գործակցի պիկերը որոշվում են կլանվող ֆոտոնի և կլանվող կամ առաքվող ֆոնոնի էներգիաների միջոցով: Ընդ որում, սպին-ուղեծրային փոխազդեցության հաշվառմամբ կամ անտեսմամբ կլանման գործակիցների արժեքների տարբերությունը առավելագույն է կլանման գործակցի՝ սպին-ուղեծրային փոխազդեցության անտեսմամբ սպացված տեղային մինիմումի տիրույթում:

Т. К. ГУКАСЯН

ОПТИЧЕСКОЕ ПОГЛОЩЕНИЕ, ОБУСЛОВЛЕННОЕ ЭЛЕКТРОН-ПОЛЯРНЫМ ОПТИЧЕСКИМ ФОНОМ И СПИН-ОРБИТАЛЬНЫМИ ВЗАИМОДЕЙСТВИЯМИ В ПОЛУПРОВОДНИКОВЫХ НАНОПРОВОЛОКАХ

Исследовано внутриподзонное и межподзонное поглощение света свободными носителями заряда в полупроводниковой нанопроволоке при рассеянии на полярных оптических фононах, опосредованное спин-орбитальными взаимодействиями Рашбы и Дрессельхауса. Зависимость коэффициента поглощения от энергии падающего фотона исследовано путем подсчета переходов между различными подзонами проводимости. Показано, что спин-орбитальное взаимодействие приводит к увеличению коэффициента внутриподзонного и межподзонного поглощения света, при этом пики коэффициента поглощения определяются энергиями поглощенного фотона и поглощенного или излученного фонона. При этом разница между значениями коэффициентов поглощения с учетом и без учета спин-орбитального взаимодействия имеет максимум в области локального минимума

коэффициента поглощения, полученного при игнорировании спин-орбитального взаимодействия.